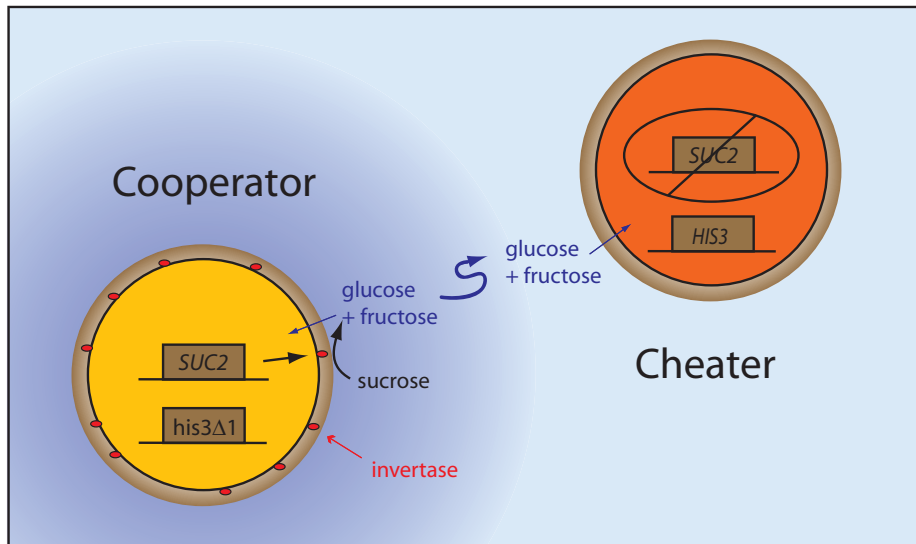
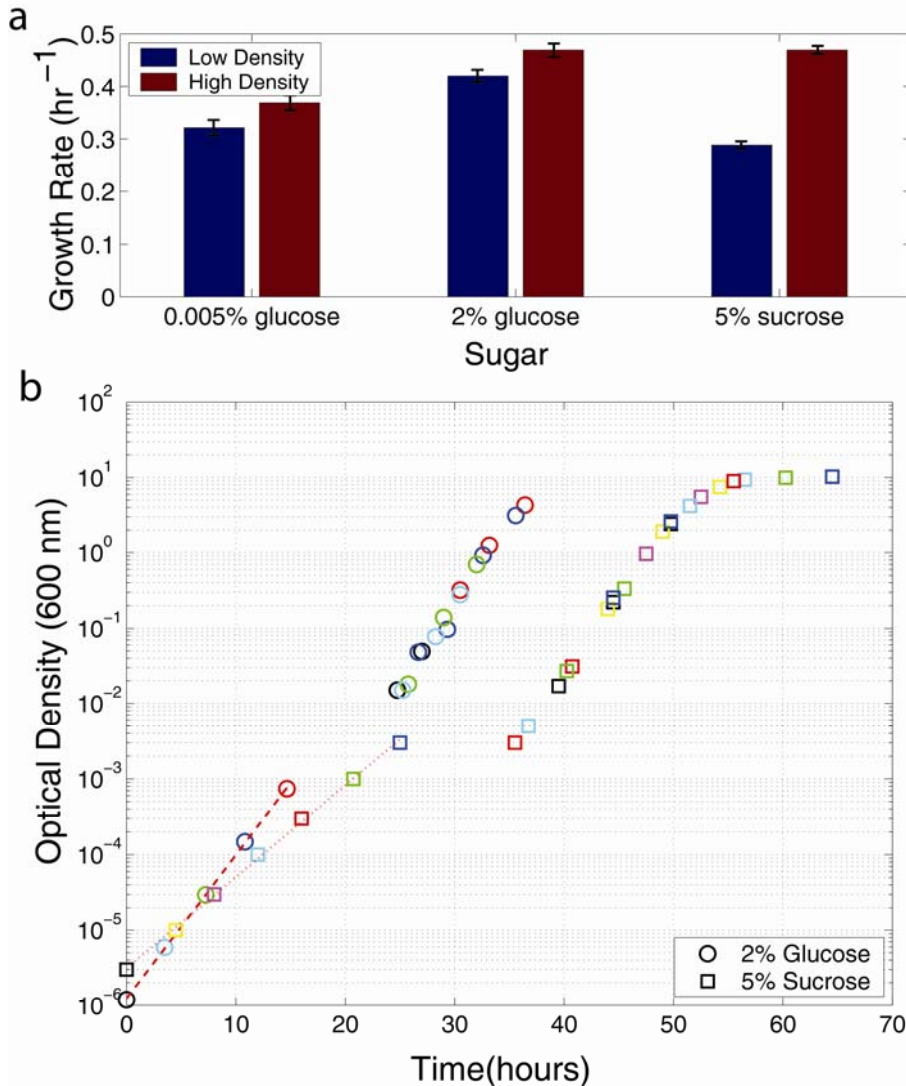


SUPPLEMENTARY INFORMATION



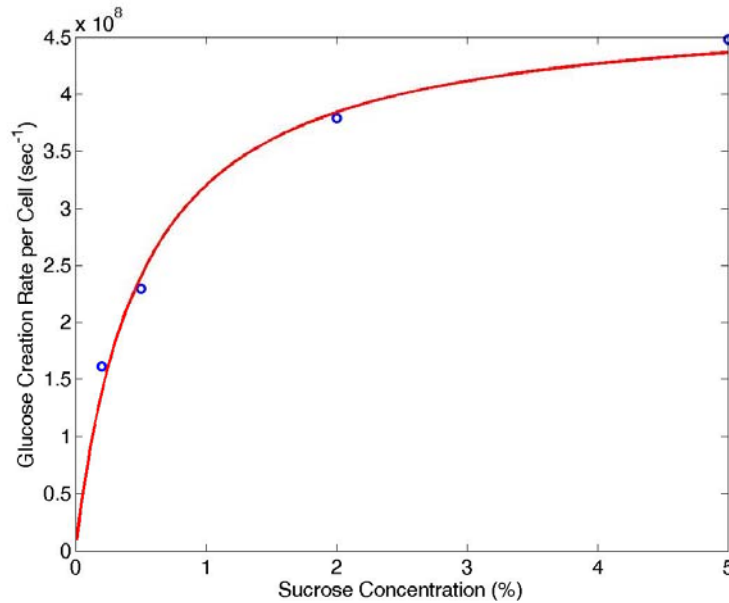
Supplementary Figure 1: Design of experiment and sucrose metabolism in yeast.

Sucrose is hydrolyzed by the enzyme invertase in the periplasmic space between the plasma membrane and the cell wall. The vast majority of the glucose and fructose created by sucrose hydrolysis diffuse away before they can be imported into the cell. This loss of sugar leads to cooperative sucrose metabolism that may be exploited by a mutant cheater strain that does not produce invertase. All strains were derived from haploid cells BY4741 (mating type **a**, EUROSCARF). The “wildtype” cooperator strain has an intact *SUC2* gene (encoding invertase), defective *HIS3* gene (*his3Δ1*), and YFP expressed constitutively by the *ADHI* promoter. The mutant cheater strain lacks the *SUC2* gene, has an intact *HIS3* gene, and has tdtomato expressed constitutively by the *PGK1* promoter. By limiting the histidine in the media we can impose a cost on the cooperator strain because it is a histidine auxotroph. The two strains can be distinguished by flow cytometry because they are expressing different fluorescent proteins.

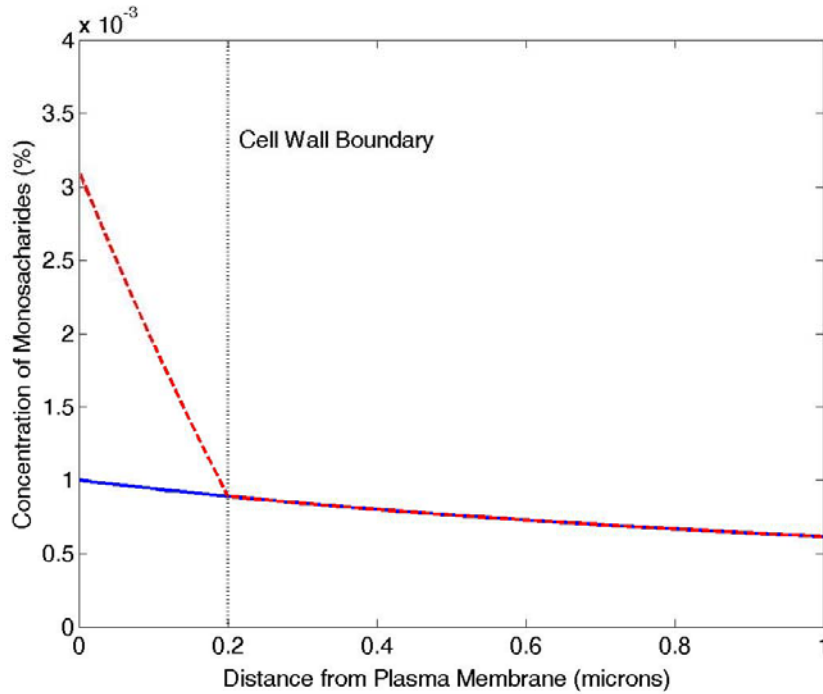


Supplementary Figure 2: Measurement of the growth rate of yeast at both low and high cell density in sucrose and glucose cultures. a, Wildtype yeast cells in 5% sucrose culture grow much faster at high cell density ($OD_{600} \geq 0.01$, red bars) than at low cell density ($OD_{600} \leq 0.001$, blue bars), an effect not observed in glucose culture. **b,** A yeast culture with Optical Density (OD, measured at 600nm) greater than ~ 0.01 can be probed accurately by absorbance in a spectrophotometer. To measure the growth rate at lower densities we used dilutions to start a set of cultures at various low optical density values and measured the time necessary for the culture to achieve a density measurable on the spectrophotometer. In the figure above we have aligned each of the resulting seven curves to overlap at high cell density (square data, 5% sucrose); the resulting location of

the starting OD values can be fit to estimate the growth rate at low density. The gap in time results from the lag phase necessary for cells to begin growth in the new media. From the average of five such experiments we estimate that the growth rate in 5% sucrose at low density ($OD < 10^{-3}$) is $\gamma_{S,low} = 0.29 \pm 0.01 \text{ hr}^{-1}$ and at high density ($OD > 0.01$) is $\gamma_{S,high} = 0.46 \pm 0.01 \text{ hr}^{-1}$ (s.e.m.). Consistent results were also obtained by direct observation of growth at low density by periodic cell plating (data not shown). Dilution experiments in glucose culture yield similar growth rates at high and low density (circles and panel a). All growth rate experiments were performed on a strain that has PSUC2:YFP in order to track invertase expression. A small amount of invertase is known to reside within the cytoplasm^{1,2} and presumably hydrolyzes any sucrose that is directly imported by the non-specific *AGT1* permease³. We find that an *AGT1* knockout strain is able to grow on sucrose in dilute cellular conditions but with a slight growth defect (~15%, data not shown), suggesting that direct sucrose import increases the effective “glucose capture efficiency”.



Supplementary Figure 3: Measurement of the glucose capture efficiency ε . Wildtype cells containing PSUC2:YFP were fully induced by growth in 0.005% glucose (see Supplementary Fig. 5a) before being transferred into media containing various sucrose concentrations. The invertase activity was quantified by measuring the appearance of glucose in the media over time using an enzymatic detection system (Sigma Glucose Assay Kit). The invertase activity per cell followed Michaelis-Menten kinetics with $V_{\max} = 4.8 \times 10^8$ monosaccharides/second and $K_m = 0.5\%$, in good agreement with published values⁴. The measured invertase activity per cell in 5% sucrose yields $V_i = (4.5 \pm 0.5) \times 10^8$ monosaccharides/second (where, in this paper, we treat fructose as being equivalent to glucose). We estimated the flux of glucose into the cell when growing on glucose by multiplying the growth rate by the number of glucose molecules required per cell (measured by observing the saturating cell density after all glucose has been consumed). In 0.003% glucose the growth rate is $0.29 \pm 0.02 \text{ hr}^{-1}$ and the cell density after all the glucose has been consumed is 2300 ± 400 cells per μL , corresponding to $\sim 4.4 \times 10^{10}$ molecules of glucose per cell. Therefore, the resulting flux in 0.003% glucose is $\mathfrak{F}_{in} = (3.5 \pm 0.9) \times 10^6$ molecules per second, and our estimate of the efficiency of glucose capture is: $\varepsilon = \frac{\mathfrak{F}_{in}}{V_i} \approx 0.01$.



Supplementary Figure 4: Diffusion analysis. By analyzing glucose diffusion at the cell surface, we can explain (1) the origin of the low glucose capture efficiency and (2) the low growth rate on sucrose in dilute cellular conditions. Invertase activity at rate V_i creates a local cloud of glucose with concentration at the cell surface⁵

$$G_{loc} \approx \frac{V_i}{4\pi D_{eff} R},$$

where $R \sim 1.6\mu\text{m}$ is the radius of the plasma membrane, $V_i = (4.5 \pm 0.5) \times 10^8$ is the invertase activity per cell, and D_{eff} is an effective diffusion constant of the monosaccharides through the cell wall and media. If we were to assume that glucose could diffuse through the cell wall unhindered then we would simply use the diffusion constant in water with 5% sucrose at 30C⁶: $D_{H2O} = 670\mu\text{m}^2/\text{sec}$. The resulting estimate of the local concentration of glucose would be $G_{loc}^* \approx 0.001\%$, about three times lower than what we infer experimentally from the growth rate in dilute cellular conditions (Supplementary Figure 2). This discrepancy could be caused by the fact that glucose diffusion through the cell wall is slower than through water.

To determine whether decreased diffusion through the cell wall might be important, we solved the diffusion equation assuming that glucose diffuses through the cell wall at a lower rate D_w . If the cell wall has radius R_w (and, therefore, thickness $R_w - R$) we find that the concentration of glucose at the plasma membrane is

$$G_{loc} = \frac{R}{R_w} \left[1 + \frac{D_{H2O}}{D_w} \left(\frac{R_w - R}{R} \right) \right] \frac{V_i}{4\pi D_{H2O} R} \equiv \frac{V_i}{4\pi D_{eff} R}$$

where we have defined an effective diffusion constant

$$\frac{1}{D_{eff}} \equiv \frac{R}{R_w} \left[\frac{1}{D_{H2O}} + \frac{1}{D_w} \left(\frac{R_w - R}{R} \right) \right]$$

Note that if the diffusion of glucose through the cell wall is the same as through water ($D_w = D$) then $D_{eff} = D$. Given that the cell wall is $\sim 200\text{nm}$ thick, the enhancement of the local concentration can be approximated as

$$\frac{G_{loc}}{G_{loc}^*} \approx 0.9 + 0.1 \frac{D_{H2O}}{D_w}$$

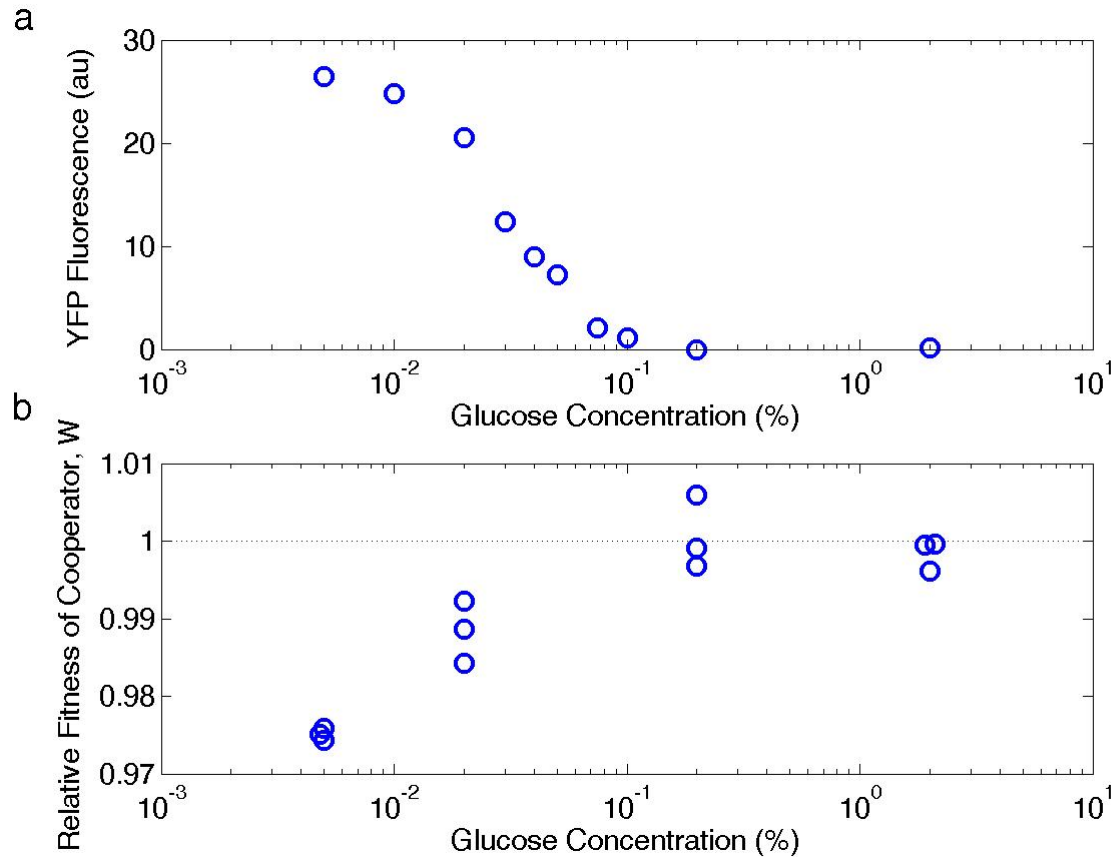
We see that the required $\sim 3\text{X}$ enhancement of the local concentration can be obtained if diffusion through the cell wall is $\sim 20\text{X}$ slower than through water [Supplementary Figure 4 plots the concentration of glucose as a function of distance from the plasma membrane assuming either no cell wall (solid blue line) or that $D_w = D_{H2O}/20$ (dashed red line)]. Given the dense interconnected nature of the cell wall, we feel that this is reasonable, although we have not been able to find experimental measurements quantifying the diffusion of small organic molecules through the yeast cell wall⁷.

Expected glucose capture efficiency: The subject of glucose import is quite complicated, but for our purposes we assume Michaelis-Menten kinetics for the net influx

$\mathfrak{S}_{in} = V_{M,t} G_{loc} / (G_{loc} + K_{M,t})$, where $V_{M,t} \approx 2 \times 10^7$ molecules/second and $K_{M,t} \sim 1\text{mM} \sim 0.02\%$ are the maximum rate and Michaelis constant for transport, respectively⁷. The expected efficiency of glucose capture is therefore consistent with our experimental measurements:

$$\varepsilon = \frac{\mathfrak{S}_{in}}{V_i} \approx \frac{V_{M,t}}{4\pi D_{eff} R K_{M,t}} \approx 0.01,$$

where we have used the fact that $G_{loc} \ll K_{M,i}$. This expression has the striking property that the fraction of glucose that is captured by the cell is *independent* of the rate of invertase activity V_i . The efficiency of glucose capture is, therefore, limited by the properties of the transporters and the nature of glucose diffusion.

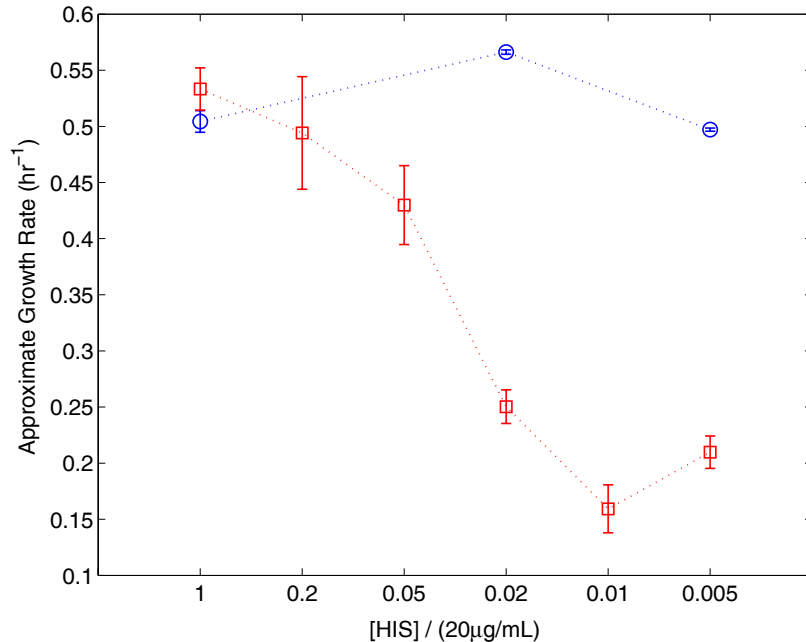


Supplementary Figure 5: Invertase expression and metabolic cost. **a**, Using a strain containing PSUC2:YFP we probed the expression of invertase as a function of the glucose concentration in the media. As expected, invertase is highly repressed at high concentrations of glucose and becomes de-repressed at lower glucose concentrations^{8,9}. This invertase expression curve allows wildtype cells to follow a strategy opposite that of their opponents (see main text). Competition experiments in this paper explored glucose concentrations in which the wildtype cells are always expressing invertase (less than or equal to 0.03%). **b**, To measure a possible metabolic cost of invertase expression we co-cultured our wildtype cooperator and mutant cheater strains in glucose culture by daily serial dilution for three days. Dilutions were performed such that the starting OD each day was ~ 0.01 , corresponding to approximately 500,000 cells. At high concentrations of glucose, when invertase is highly repressed, the two strains grew at similar rates. At low concentration of glucose the cooperator strain began expressing invertase and had a growth deficit of $\sim 2.5\%$ relative to the cheater strain. This result is consistent with a

metabolic cost of invertase production and secretion. The values plotted correspond to the relative fitness of the cooperator compared to the cheater¹⁰:

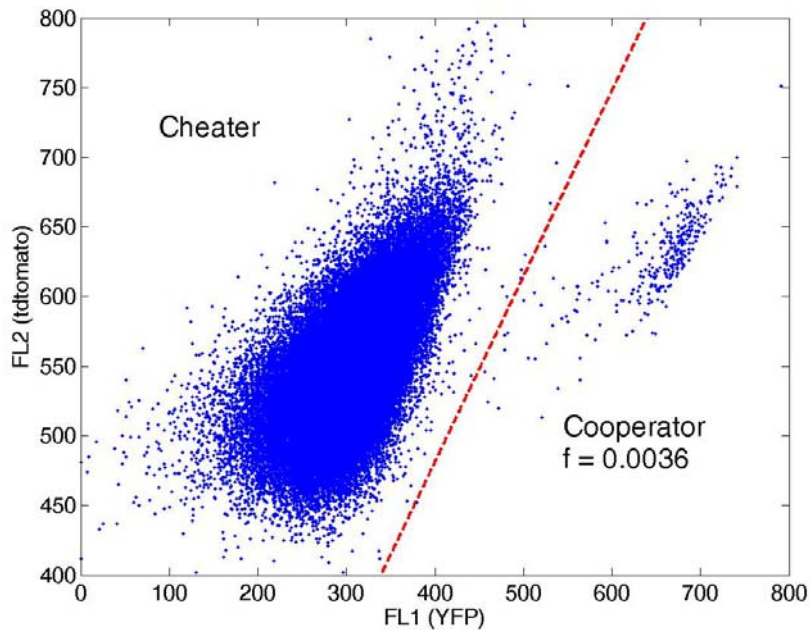
$$W = \ln \left[\frac{OD_f f_f}{OD_i f_i} \right] / \ln \left[\frac{OD_f (1 - f_f)}{OD_i (1 - f_i)} \right],$$

where f_i and f_f are the initial and final fraction of cooperator and OD_i and OD_f are the initial and final cell density (taking into account the daily serial dilutions).

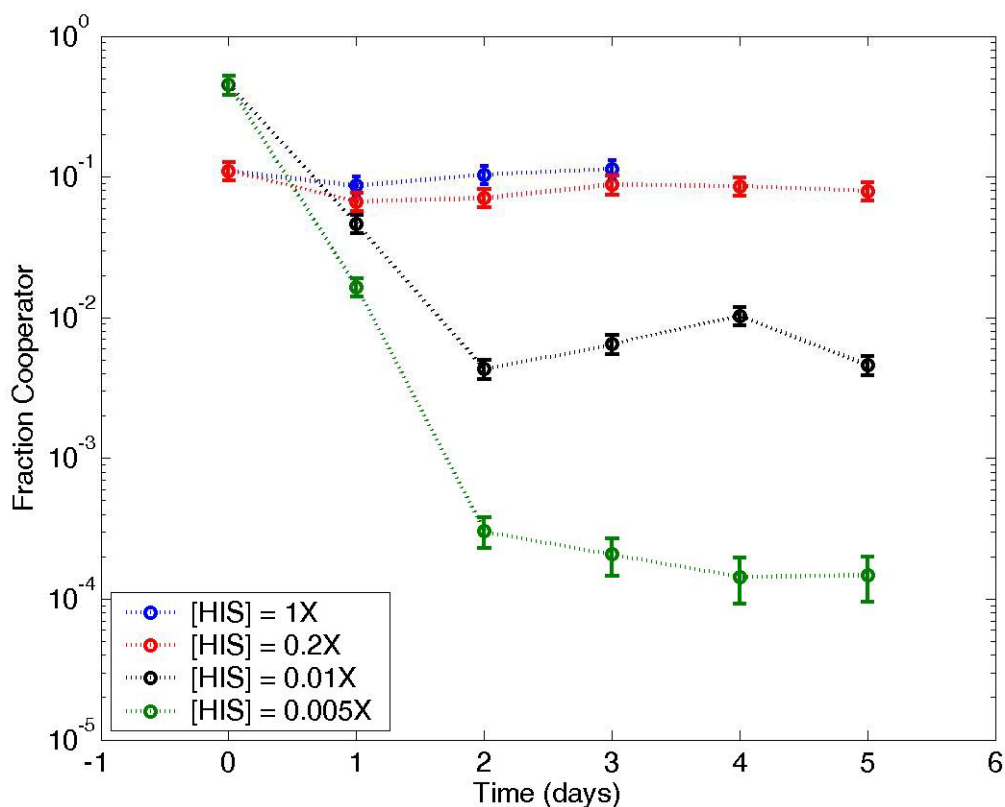


Supplementary Figure 6: Growth rate of cooperator (red squares) and cheater (blue circles) strains as a function of the histidine concentration in the media.

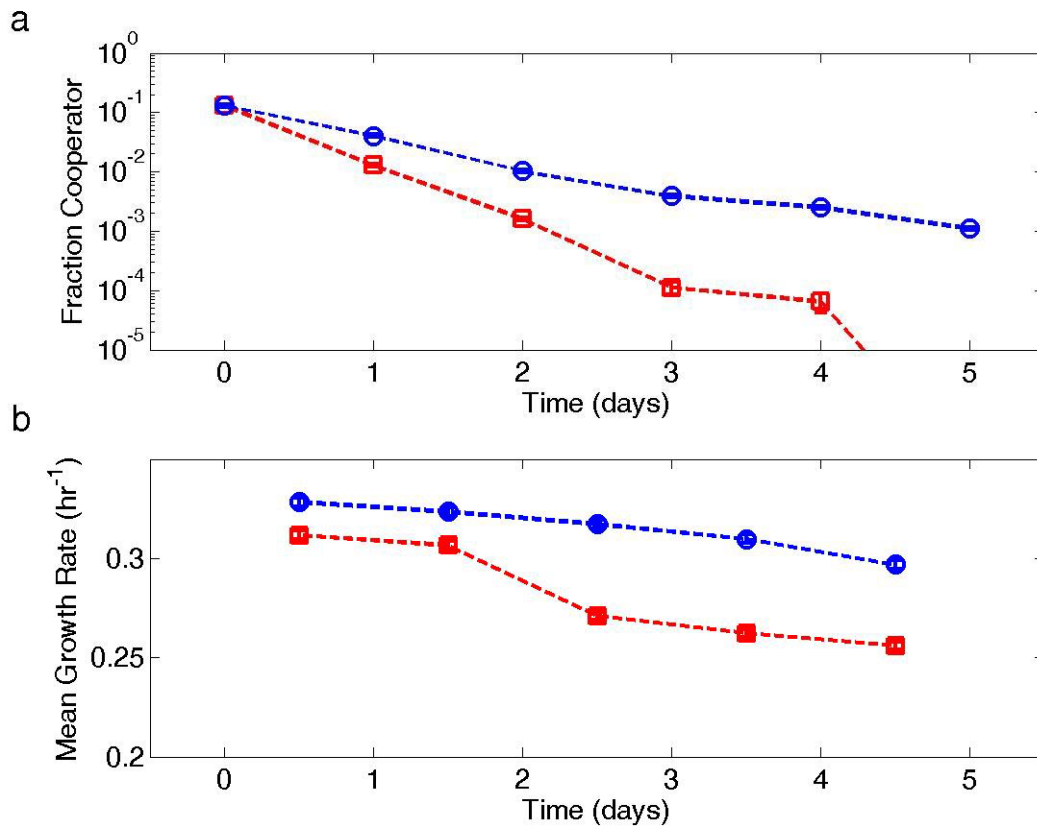
Growth rate during exponential phase was measured in minimal media containing 2% glucose and supplemented with the indicated concentration of histidine (error bars indicate s.e.m. of two or more measurements). The growth rate of the cheater strain is not sensitive to the histidine concentration because the strain contains an intact histidine synthesis pathway. However, the cooperator is a histidine auxotroph and therefore grows more slowly at lower concentrations of histidine. Histidine limits both the growth rate and the total density of the cooperator, although during competition experiments most of the growth occurs at low cell density such that only the first effect is acting. We find that the cooperator (histidine auxotroph) can grow to a maximum cell density of $OD \sim 10 * [\text{histidine}]/(20\mu\text{g/mL})$ before exhausting the histidine in the media. The low final density at low histidine concentrations limited the accuracy with which we could measure the growth rate of the cooperator strain.



Supplementary Figure 7: Distinguishing the two strains by flow cytometry. The “cooperator” strain has YFP expressed constitutively by the ADH1 promoter and the “cheater” strain has tdtomato expressed constitutively by the PGK1 promoter. We distinguish the two strains using a Becton Dickinson FACScan flow cytometer with excitation laser at 488nm. Emission filter FL1 (530/30) detects YFP levels and FL2 (585/42) detects tdtomato levels, although the absorbance of tdtomato at 488nm is relatively inefficient. The plot above is from a sample after competition has been allowed to proceed to equilibrium in 0.01X HIS, 5% sucrose, and 0.001% glucose. The two strains are distinguished using a combination of the signal in FL1 and FL2 (red dashed line). The dashed line above identifies 312 cooperators out of a total of 87,619 cells, yielding an estimate of $f = 0.0036$ as the fraction of cooperators at equilibrium. The cutoff was adjusted slightly for each sample, but the dashed line above gives a false positive rate for identifying cooperators of less than 10^{-4} (more stringent cutoffs were used for smaller fractions of cooperator). We believe that the error in our measurements of the cooperative fraction is generally larger than the binomial counting error (which is often very small given that we typically count $\sim 100,000$ cells). In Figures 1a,b and 3a we therefore plot an error bar that is the larger of 1) the binomial counting error or 2) the variation in measured fractions that we get by the range of reasonable threshold values (roughly 10 - 15%).



Supplementary Figure 8: Coexistence between the wildtype cooperator and mutant cheater is also observed in continuous culture. We employed a home-built turbidostat¹¹ to compete our two strains in continuous culture. The turbidostat maintains the co-culture at constant turbidity (cell density). The experiments above were performed in a 10mL culture at a constant optical density (OD) of approximately 0.15 with 2% sucrose and variable histidine concentrations. As expected, the fraction of cooperators at equilibrium decreases as the histidine concentration is decreased (causing the cost of cooperation to increase). The fractions of the two strains were measured by flow cytometry each day. Turbidostat cultures typically flocculated after a few days, thus limiting the length of experiments (particularly at high histidine concentrations).

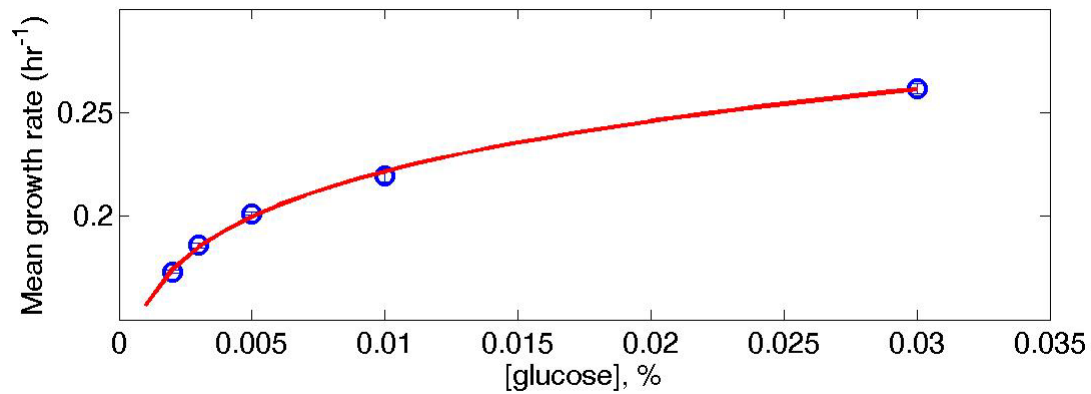


Supplementary Figure 9: Evolution of a competing culture can lead to decreasing growth rates. Two cultures in 5% sucrose and 0.03% glucose were started with an initial fraction of 13% cooperators. Over time both the 0.2X HIS (blue circle) and 0.05X HIS (red square) cultures had a decrease in the fraction of cooperators (a) and the growth rate (b). The decreasing fitness over time is a striking manifestation of the cooperative interaction, as evolutionary dynamics normally lead to an increase in the mean fitness of a population¹².

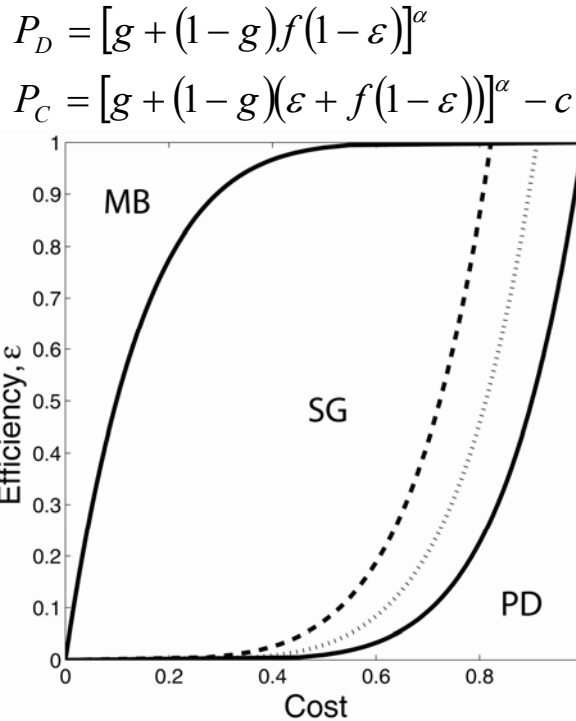
	Opp (coop)	Opp (def)
You (coop)	R	S
You (defect)	T	P

Game	Condition	Optimal Strategy	Outcome
Mutually Beneficial	$R > T, S > P$	Cooperation	Cooperators win
Snowdrift Game	$T > R > S > P$	Opposite of opponent	Coexistence
Coordination Game	$R > P > T, S$	Same as opponent	History dependent
Prisoner's Dilemma	$T > R > P > S$	Defect	Defectors win

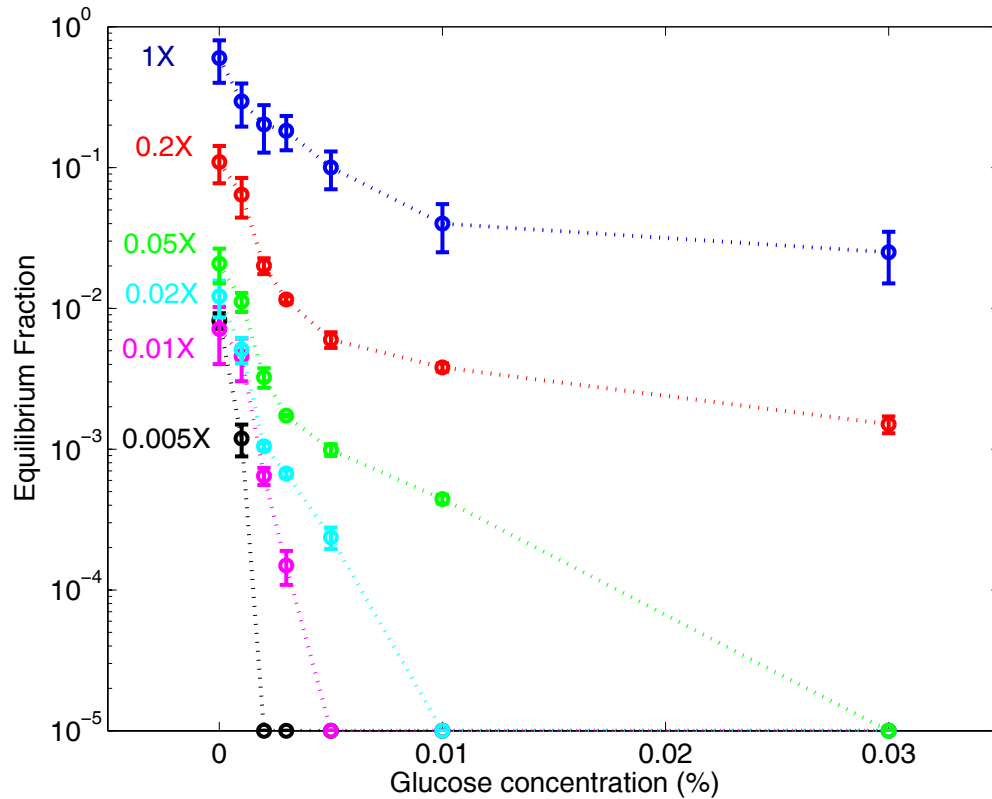
Supplementary Table 1: Summary of symmetric two-person game theory models of cooperation. The matrix shows the payout to you based on your strategy and the strategy followed by your opponent. The outcome of competition in a well-mixed environment is determined by the relative ordering of R, S, T, and P (in order for this to be a model of cooperation, we require $R > P$). The net payout to an individual in a population in a well-mixed environment is then typically the sum of all the pairwise payouts. The nonlinear model in Figure 2b is able to generate interactions equivalent to all four of the common game theory models of cooperation¹³. The coordination game (also known as the stag hunt game¹⁴) is obtained for $\alpha > 1$ in the region of intermediate cost c and efficiency ϵ . In the coordination game, a population of cooperators is non-invasible by a cheater and a population of cheaters is non-invasible by a cooperator. Thus, the outcome of such competition is history-dependent.



Supplementary Figure 10: Measurement of nonlinear benefits. The cheater strain was grown in 5% sucrose plus various concentrations of glucose for 23 hours from an initial Optical Density of 0.0025 (same conditions as our competition experiments but without the cooperator strain; note that the sucrose is not hydrolyzed). The mean growth rate is shown together with the power law fit, yielding $\alpha = 0.15 \pm 0.01$.



Supplementary Figure 11: Extension of the basic nonlinear model in Figure 2b to include the effect of glucose in the media. We maintain the normalization of unity and allow growth based on either the benefits of cooperation or from glucose in the media (g). As glucose is added to the system, the boundary between the snowdrift game (SG) and the prisoner's dilemma (PD) shifts to the left. The boundary line is defined by the equation $(g + (1 - g)\varepsilon)^\alpha - c = g^\alpha$ because, when this condition is satisfied, a cooperator and cheater do equally well in a population of cheaters. In the figure above, we plot this boundary for $g = 0$ (solid line), $g = 10^{-7}$ (dotted line) and $g = 10^{-5}$ (dashed line). Note that the glucose concentration at which the cooperators go extinct will be a decreasing function of the cost of cooperation, an effect that we observe experimentally (Fig. 3b).



Supplementary Figure 12: Fraction of cooperators at equilibrium as a function of glucose and histidine concentration. All cultures had 5% sucrose (1X HIS = 20 μ g/mL). This data was used to construct Figure 3b (error bars are s.e.m., two or three independent experiments). A measured fraction $f < 3 \times 10^{-5}$ was assumed to correspond to extinction of cooperator and is plotted as $f = 10^{-5}$ in the figure above and in Figure 3b. Our 5% sucrose media typically had monosaccharides present at $\sim 0.0001\%$. Variation in this concentration made the “0% glucose” data somewhat less reproducible than the other data points.

References

1. Perlman, D. & Halvorson, H.O. Distinct Repressible Messenger-Rnas for Cytoplasmic and Secreted Yeast Invertase Are Encoded by a Single Gene. *Cell* **25**, 525-536 (1981).
2. Carlson, M. & Botstein, D. 2 Differentially Regulated Messenger-Rnas with Different 5' Ends Encode Secreted and Intracellular Forms of Yeast Invertase. *Cell* **28**, 145-154 (1982).
3. Stambuk, B.U., da Silva, M.A., Panek, A.D. & de Araujo, P.S. Active alpha-glucoside transport in *Saccharomyces cerevisiae*. *Fems Microbiology Letters* **170**, 105-110 (1999).
4. Vitolo, M. & Yassuda, M.T. Effect of Sucrose Concentration on the Invertase Activity of Intact Yeast-Cells (*Saccharomyces-Cerevisiae*). *Biotechnology Letters* **13**, 53-56 (1991).
5. Berg, H.C. *Random Walks in Biology*, (Princeton University Press, Princeton, NJ, 1993).
6. Weast, R. *CRC Handbook of Chemistry and Physics*, (CRC Press, Inc., Boca Raton, Florida, 1984).
7. Dickinson, J.R. & Schweizer, M. *The Metabolism and Molecular Physiology of Saccharomyces cerevisiae*, (CRC Press, Boca Raton, FL, 2004).
8. Gancedo, J.M. Yeast carbon catabolite repression. *Microbiology and Molecular Biology Reviews* **62**, 334-361 (1998).
9. Ozcan, S., Vallier, L.G., Flick, J.S., Carlson, M. & Johnston, M. Expression of the SUC2 gene of *Saccharomyces cerevisiae* is induced by low levels of glucose. *Yeast* **13**, 127-137 (1997).
10. Greig, D. & Travisano, M. The Prisoner's Dilemma and polymorphism in yeast SUC genes. *Proceedings of the Royal Society of London Series B-Biological Sciences* **271**, S25-S26 (2004).
11. Acar, M., Mettetal, J.T. & van Oudenaarden, A. Stochastic switching as a survival strategy in fluctuating environments. *Nature Genetics* **40**, 471-475 (2008).
12. Nowak, M.A. *Evolutionary Dynamics*, (Belknap Press, Cambridge, MA, 2006).
13. Doebeli, M. & Hauert, C. Models of cooperation based on the Prisoner's Dilemma and the Snowdrift game. *Ecology Letters* **8**, 748-766 (2005).
14. Skyrms, B. *The Stag Hunt and Evolution of Social Structure*, (Cambridge University Press, Cambridge, 2004).